A Monte Carlo Simulation of Polymer–Polymer Interdiffusion

Wolfgang Jilge,[†,‡] I. Carmesin,[‡,§] Kurt Kremer,*[,∥] and Kurt Binder[‡]

Institut für Physik, Johannes-Gutenberg-Universität Mainz, Staudinger Weg 7, D-6500 Mainz, Federal Republic of Germany, Max-Planck-Institut für Polymerforschung, Postfach 3148, D-6500 Mainz, Federal Republic of Germany, Institut für Festkörperforschung, KFA Jülich, Postfach 1913, D-5170 Jülich, Federal Republic of Germany, and Bayer AG, D-5090 Leverkusen, Federal Republic of Germany

Received December 5, 1989; Revised Manuscript Received April 7, 1990

ABSTRACT: The interdiffusion of fully compatible symmetric binary (AB) polymer mixtures, which are prepared in a thin film geometry where a film of pure polymer A is coated with a film of pure polymer B, is studied by Monte Carlo simulation. The time dependence of the concentration profiles is studied for chain lengths $N = 10, 20$ and three ratios of the monomer mobilities $\Gamma_A/\Gamma_B = 1, 0.5$, and 0.1 and two melt densities. Also the related problem of small-molecule interdiffusion ($N = 1$) is studied for comparison. The tracer diffusion coefficients are obtained from the time dependence of mean-square displacements of the center of gravity of the chains, and thus approximate theories relating self-diffusion and interdiffusion can be tested. The phenomenological theories based on the vacancy model of polymer–polymer interdiffusion are described briefly. It is argued, however, that a simple relation between the interdiffusion coefficient and the tracer diffusion constants does not exist.

1. Introduction

Interdiffusion of macromolecules in polymer blends has become the subject of both theoretical[1-16] and experimental[16-28] research recently. In fact, mutual diffusion of polymers may even be technologically important for the processing of incompatible polymer mixtures, for crack healing in glassy polymers,[29] etc. It is also a problem of fundamental interest, linking together thermodynamic and kinetic properties of the blend.

Thus one of the key ideas of the theories[1-16] has been to express the interdiffusion coefficient, D_{int}, of a polymer mixture as a product of a "thermodynamic factor", which depends on static properties only, and a "kinetic factor", which involves friction coefficients characterizing the diffusion of the two types of chains but is not dependent on the effective interactions described, e.g., by the Flory–Huggins χ-parameter.[30] Since various techniques exist[16] to measure self-diffusion coefficients in polymer melts, any relation expressing the interdiffusion coefficient in such a form where the "kinetic factor" is a simple function of the self-diffusion coefficients D_A^* and D_B^* of the constituents of the AB mixture would be of great practical interest: one could theoretically predict the temperature and composition dependence of the interdiffusion coefficient, once the thermodynamic properties of the blend and these self-diffusion coefficients are known. Thus, a number of approximate theories has considered this problem and relations have been suggested,[3-13] although the insight is growing[14-16] that a simple relation between self-diffusion and interdiffusion coefficients should not exist.

The various theoretical treatments predicting such a simple relation[3-13] are not in mutual agreement with each other either: for a noninteracting binary (A,B) mixture of chains with chain lengths N_A and N_B and with volume fractions ϕ_A and ϕ_B the "slow mode" theory predicts[3-5,9,10,12]

$$D_{int}^{-1} = [(N_A D_A^* \phi_A)^{-1} + (N_B D_B^* \phi_B)^{-1}]/[(N_A \phi_A)^{-1} + (N_B \phi_B)^{-1}] \quad (1)$$

while the "fast mode" theory predicts[6,7,11]

$$D_{int} = \phi_A \phi_B [(N_A D_A^* \phi_B) + (N_B D_B^* \phi_A)][(N_A \phi_A)^{-1} + (N_B \phi_B)^{-1}] \quad (2)$$

In a dense incompressible melt, to which these expressions apply, one takes $\phi_A + \phi_B = 1$, but we shall later consider a more general compressible case, which in the framework of a lattice model is accounted for by a volume fraction ϕ_V of vacancies ($\phi_A + \phi_B = 1 - \phi_V$).

From eqs 1 and 2 we see that, for the case where one species is much faster diffusing than the other ($D_A^* \gg D_B^*$), eq 1 predicts that interdiffusion is controlled by the slow component $\{D_{int} \approx D_B^*[(N_B\phi_B)/(N_A\phi_A) + 1]\}$ while eq (2) predicts interdiffusion to be controlled by the fast component $\{D_{int} \approx D_A^* \phi_B^2 [1 + (N_A\phi_A)/(N_B\phi_B)]\}$. Note that for the case where one species gets very dilute ($\phi_A \to 0$) we get from both expressions the same result, $D_{int} \approx D_A^*$: thus D_A^* and D_B^* in eqs 1 and 2 really should be interpreted as the self-diffusion coefficients of an A chain in a B matrix and of a B chain in an A matrix and not as the self-diffusion coefficients of the chains in pure melts of the same kind. Finally, we recall that in the symmetric case $N_A = N_B = N$ eqs 1 and 2 reduce to the simple expression

$$D_{int}^{-1} = \phi_B/D_A^* + \phi_A/D_B^* \quad \text{slow mode theory} \quad (3)$$

$$D_{int} = \phi_B D_A^* + \phi_A D_B^* \quad \text{fast mode theory} \quad (4)$$

Equations 1 and 3 disregard bulk flow, and hence a fast chain can take a volume region previously taken by a slow chain if the latter diffuses away, in order to give rise to interdiffusion. The opposite result of eqs 2 and 4 is attributed to bulk flow.[6,16]

A number of studies have then attempted to distinguish between eqs 3 and 4 by experiment and thus settle this issue. Of course, real mixtures are always to some extent interacting, and thus the thermodynamic factor $[(N_A\phi_A)^{-1} + (N_B\phi_B)^{-1}]$ in eqs 1 and 2 has to be replaced by $[(N_A\phi_A)^{-1} + (N_B\phi_B)^{-1} - 2\chi]$, with χ being the Flory–Huggins parameter,[30] which itself is temperature- and concentration-dependent.[31] Apart from this difficulty, it is not straightforward to test eqs 1–4: one cannot assume that D_A^* and D_B^* are independent of volume fraction, apart from the

* To whom correspondence should be addressed.
† Present and permanent address: Bayer AG.
‡ Johannes-Gutenberg-Universität Mainz.
§ Max-Planck-Institut für Polymerforschung.
∥ KFA Jülich.

0024-9297/90/2223-5001$02.50/0

dilute limit, where both expressions 1 and 2 become identical, however. Thus some of the experiments (refs 18, 21, 23–25, 27, and 28 claim evidence for the slow mode theory while refs 19, 20, 22, and 26 claim to prove the fast mode theory) certainly are not very conclusive; in addition, the possibility that neither eq 1 nor 2 holds true also must be seriously considered.[15]

In this situation, it is attractive to study this problem by computer simulation; here it is trivial to have a strictly noninteracting (athermal) case, and D_A^*, D_B^*, and D_{int} can directly be obtained from the simulation. Of course, the computer simulation deals with a specific microscopic model, and the question must be raised whether the model captures the essential features of the real materials. Since the present work restricts attention to lattice models of macromolecules, where one has an ideal and rigid lattice from the outset, and hydrodynamic fluidlike behavior cannot occur, the answer to this question certainly is nontrivial. Nevertheless, some formulations of the theory, such as refs 3, 4, 6, 9, and 10, should encompass this model, and hence the validity of such theories is tested in a nontrivial manner.

The outline of this paper is as follows. Section 2 summarizes the phenomenological theory describing interdiffusion of polymers in the framework of a dynamic version of the Flory–Huggins lattice model. Although this treatment is restricted to diffusion via a vacancy mechanism, both eqs 1 and 2 can be obtained from it by various assumptions, the validity of which we want to investigate. Section 3 then describes the model studied in the simulations and discusses some technical aspects of these simulations. Section 4 describes our simulation results on interdiffusion, while section 5 analyzes the time dependence of mean-square displacements and the resulting self-diffusion coefficients. Section 6 then compares our results to the simple predictions, eqs 1–4, and briefly summarizes our conclusions. Also brief indications are given on the directions where future research along similar lines will be useful, and possible consequences for the interpretation of experimental data will be discussed.

2. Phenomenological Theory of Interdiffusion in Dynamic Flory–Huggins Lattice Models of Polymer Blends

We consider a lattice where each site may be taken by either a segment of an A polymer or a segment of a B polymer, or by a vacancy V, and describe interdiffusion in the framework of Onsager's linearized nonequilibrium transport theory. Related treatments have recently been given for lattice gases;[15] there any aspects specific to polymers are missing. For the polymer case always nondiagonal Onsager coefficients are disregarded from the start.[9,10,12] In view of the recent work on lattice gases,[15] one must suspect that the latter assumption is rather inappropriate. In this paper, it was shown by direct "measurement" of both diagonal and off-diagonal Onsager coefficients and the interdiffusion constant that all Onsager coefficients actually are comparable in magnitude and are needed for a quantitative theory of interdiffusion. Therefore, it is worthwhile to present a treatment that is completely general, containing both the lattice gas limit[15] and the previous work on polymers with only diagonal Onsager coefficients as special cases. In this way, a coupled system of diffusion equations is obtained, which should be capable to describe computer simulations as well as real experiments.

Each of the N lattice sites can be taken once, and we have a total number n_A of monomers of species A, a total number n_B of species B, and n_V vacant sites (with $n_A + n_B + n_V = N$). We define volume fractions ϕ_A, ϕ_B, and ϕ_V as

$$\phi_A = n_A/N, \quad \phi_B = n_B/N, \quad \phi_V = n_V/N \tag{5}$$

with

$$\phi_A + \phi_B + \phi_V = 1 \tag{6}$$

Static properties are described within the mean-field limit by the Flory–Huggins free energy f per lattice site

$$f = F/N = \left\{ k_B T \frac{\phi_A}{N_A} \ln \phi_A + \frac{\phi_B}{N_B} \ln \phi_B + \phi_V \ln \phi_V + \frac{1}{2}\chi_{AA}\phi_A^2 + \frac{1}{2}\chi_{BB}\phi_B^2 + \frac{1}{2}\chi_{VV}\phi_V^2 + \chi_{AB}\phi_A\phi_B + \chi_{AV}\phi_A\phi_V + \chi_{BV}\phi_B\phi_V \right\} \tag{7}$$

Here k_B is the Boltzmann's constant, and T is the absolute temperature, and the first three terms are the familiar entropy of mixing terms, while the remaining most general quadratic form in the ϕ's represents the effective enthalpic contribution. Here χ_{AA}, χ_{BB}, χ_{VV}, χ_{AB}, χ_{AV}, and χ_{BV} are suitable functions, which themselves may depend on the volume fractions and on temperature. In the "noninteracting" case mentioned in the introduction, all these enthalpic terms are put equal to zero.

Dynamics are introduced into this model by suitable jumps of monomers to neighboring sites (for an explicit realization of an actual algorithm, realizing these motions in the simulations, see section 3). Since the numbers n_A, n_B, and n_V are conserved by this process, we have three conservation laws expressed in terms of the continuity equations

$$\frac{\partial \phi_A(\vec{r},t)}{\partial t} + \nabla \cdot \vec{j}_A(\vec{r},t) = 0 \tag{8a}$$

$$\frac{\partial \phi_B(\vec{r},t)}{\partial t} + \nabla \cdot \vec{j}_B(\vec{r},t) = 0 \tag{8b}$$

$$\frac{\partial \phi_V(\vec{r},t)}{\partial t} + \nabla \cdot \vec{j}_V(\vec{r},t) = 0 \tag{8c}$$

where from the lattice via suitable coarse-graining we have defined volume fraction fields $\phi_A(\vec{r},t)$, $\phi_B(\vec{r},t)$, and $\phi_V(\vec{r},t)$ depending on position $\vec{r}$ in continuous space and on time t. Owing to eq 6, the current densities $\vec{j}_A(\vec{r},t)$, $\vec{j}_B(\vec{r},t)$, and $\vec{j}_V(\vec{r},t)$ of monomers A, monomers B, and vacancies are not independent of each other but rather are coupled by the relation

$$\nabla \cdot [\vec{j}_A(\vec{r},t) + \vec{j}_B(\vec{r},t) + \vec{j}_V(\vec{r},t)] = 0 \tag{9a}$$

and since we disregard both uniform and rotational flow patterns, this implies

$$\vec{j}_A(\vec{r},t) + \vec{j}_B(\vec{r},t) + \vec{j}_V(\vec{r},t) = 0 \tag{9b}$$

It is instructive to note that at this point we already differ from the treatment presented by Kramer et al.,[6] who at the same time imply that vacancies can be created and destroyed rapidly—i.e., vacancies are not conserved—but still assume eq 9b, which only follows if vacancies are conserved.

Here it is important to mention the limitations of our approach. The theory is still on a mean-field level. This means that excluded volume is not explicitly taken into account. There is only a global volume conservation. The chain dynamics itself is treated only on the level of the simple Rouse model, neglecting all further possible

complications (e.g., reptation for long chains or hydrodynamics for larger ϕ_V). Nevertheless it is obvious from ref 15 that even on this level of the description it is important to consistently take into account the various relative mobilities of the species in order to obtain a coherent picture.

Now the Onsager formalism[32-34] amounts to postulate constitutive equations relating linearly the current densities to the gradients of the chemical potentials μ_A, μ_B, and μ_V of monomers of species A, monomers of species B, and vacancies V:

$$k_BT\vec{j}_A = -\Lambda_{AA}\nabla\mu_A - \Lambda_{AB}\nabla\mu_B - \Lambda_{AV}\nabla\mu_V \quad (10a)$$

$$k_BT\vec{j}_B = -\Lambda_{BA}\nabla\mu_A - \Lambda_{BB}\nabla\mu_B - \Lambda_{BV}\nabla\mu_V \quad (10b)$$

$$k_BT\vec{j}_V = -\Lambda_{VA}\nabla\mu_A - \Lambda_{VB}\nabla\mu_B - \Lambda_{VV}\nabla\mu_V \quad (10c)$$

These equations define the Onsager coefficients Λ_{ij}. However, not all of these coefficients are independent of each other: the Onsager reciprocity relations yield

$$\Lambda_{BA} = \Lambda_{AB}, \quad \Lambda_{AV} = \Lambda_{VA}, \quad \Lambda_{BV} = \Lambda_{VB} \quad (11)$$

and the condition eq 9b that the total current vanishes requires

$$(\Lambda_{AA} + \Lambda_{BA} + \Lambda_{VA})\nabla\mu_A + (\Lambda_{AB} + \Lambda_{BB} + \Lambda_{VB})\nabla\mu_B + (\Lambda_{AV} + \Lambda_{BV} + \Lambda_{VV})\nabla\mu_V = 0 \quad (12)$$

Since eq 12 must be true for arbitrary chemical potentials μ_A, μ_B, and μ_V, the expressions in brackets in eq 12 must vanish individually, which yields together with eq 11

$$\Lambda_{AV} = -(\Lambda_{AA} + \Lambda_{AB}) \quad (13a)$$

$$\Lambda_{BV} = -(\Lambda_{AB} + \Lambda_{BB}) \quad (13b)$$

$$\Lambda_{VV} = -(\Lambda_{AV} + \Lambda_{BV}) = \Lambda_{AA} + 2\Lambda_{AB} + \Lambda_{BB} \quad (13c)$$

Equations 10, 11, and 13 imply that the monomer current densities $\vec{j}_A$ and $\vec{j}_B$ become

$$\vec{j}_A = -(\Lambda_{AA}/k_BT)\nabla(\mu_A - \mu_V) - (\Lambda_{AB}/k_BT)\nabla(\mu_B - \mu_V) \quad (14a)$$

$$\vec{j}_B = -(\Lambda_{BA}/k_BT)\nabla(\mu_A - \mu_V) - (\Lambda_{BB}/k_BT)\nabla(\mu_B - \mu_V) \quad (14b)$$

These equations differ from previous work[6,10,12] because they contain the nondiagonal terms coupling the A current also to a chemical potential gradient between B monomers and vacancies and the B current to a chemical potential gradient between A monomers and vacancies. While in ref 6 it was additionally assumed that the vacancies attain local equilibrium instantaneously and hence $\nabla\mu_V = 0$, we here rather use eq 7 to obtain the chemical potentials in a thermodynamically consistent fashion[10,12] from $\mu_i = \partial F/\partial n_i|_{T,N_{j\neq i}}$. Using $F = Nf$ and differentiating with respect to the ϕ_i yields

$$\mu_i = \sum_j (\partial f/\partial\phi_j)(\delta_{ij} - \phi_j) \quad (15)$$

where the sums run over A, B, and V, and three chemical potentials appear since in eq 15 we consider the n_A, n_B, and n_V as independently varying quantities. The three chemical potentials are not independent of each other, however, due to the Gibbs–Duhem relation, which follows from eq 15

$$f = \mu_A\phi_A + \mu_B\phi_B + \mu_V\phi_V \quad (16)$$

Comparing the differential $df = -s\,dT + \sum_i(\partial f/\partial\phi_i)\,df_i$, where s is the entropy density, with the explicit differential of eq 16, we can also derive a differential form of the Gibbs–Duhem relation, for isothermal processes ($dT = 0$)

$$\phi_A\,d\mu_A + \phi_B\,d\mu_B + \phi_V\,d\mu_V = 0 \quad (17)$$

In our model it hence is not consistent to require $\nabla\mu_V = 0$, because $\nabla\mu_V$ is related to $\nabla\mu_A$ and $\nabla\mu_B$ via eq 17.

Using now the explicit form of f (eq 7), we obtain from eq 15 for the required chemical potential differences

$$\frac{\mu_A - \mu_V}{k_BT} = \frac{\ln\phi_A + 1}{N_A} + \chi_{AA}\phi_A + \chi_{AB}\phi_B + \chi_{AV}\phi_V - [\chi_{AV}\phi_A + \chi_{BV}\phi_B + \chi_{VV}\phi_V + \ln\phi_V] \quad (18a)$$

$$\frac{\mu_B - \mu_V}{k_BT} = \frac{\ln\phi_B + 1}{N_B} + \chi_{BB}\phi_B + \chi_{AB}\phi_A + \chi_{BV}\phi_V - [\chi_{AV}\phi_A + \chi_{BV}\phi_B + \chi_{VV}\phi_V + \ln\phi_V] \quad (18b)$$

Using now eqs 18a and b in eqs 14a and b and eliminating $\nabla\phi_V = -\nabla\phi_A - \nabla\phi_B$ (which follows from eq 6) yields the desired expressions for the current densities

$$\vec{j}_A(\vec{r},t) = -D_{AA}(\phi_A,\phi_B)\nabla\phi_A(\vec{r},t) - D_{AB}(\phi_A,\phi_B)\nabla\phi_B(\vec{r},t) \quad (19a)$$

$$\vec{j}_B(\vec{r},t) = -D_{BA}(\phi_A,\phi_B)\nabla\phi_A(\vec{r},t) - D_{BB}(\phi_A,\phi_B)\nabla\phi_B(\vec{r},t) \quad (19b)$$

where four diffusion coefficients enter, which are given as follows:

$$D_{AA}(\phi_A,\phi_B) = \Lambda_{AA}(\phi_A,\phi_B)\left[\frac{1}{\phi_A N_A} + \frac{1}{\phi_V} + \chi_{AA} + \chi_{VV} - 2\chi_{AV}\right] + \Lambda_{AB}(\phi_A,\phi_B)\left[\frac{1}{\phi_V} + \chi_{AB} + \chi_{VV} - \chi_{AV} - \chi_{BV}\right] \quad (20a)$$

$$D_{AB}(\phi_A,\phi_B) = \Lambda_{AA}(\phi_A,\phi_B)\left[\frac{1}{\phi_V} + \chi_{AB} + \chi_{VV} - \chi_{AV} - \chi_{BV}\right] + \Lambda_{AB}(\phi_A,\phi_B)\left[\frac{1}{N_B\phi_B} + \frac{1}{\phi_V} + \chi_{BB} + \chi_{VV} - 2\chi_{BV}\right] \quad (20b)$$

$$D_{BA}(\phi_A,\phi_B) = \Lambda_{AB}(\phi_A,\phi_B)\left[\frac{1}{N_A\phi_A} + \frac{1}{\phi_V} + \chi_{AA} + \chi_{VV} - 2\chi_{AV}\right] + \Lambda_{BB}(\phi_A,\phi_B)\left[\frac{1}{\phi_B} + \chi_{AB} + \chi_{VV} - \chi_{AV} - \chi_{BV}\right] \quad (20c)$$

and

$$D_{BB}(\phi_A,\phi_B) = \Lambda_{AB}(\phi_A,\phi_B)\left[\frac{1}{\phi_V} + \chi_{AB} + \chi_{VV} - \chi_{AV} - \chi_{BV}\right] + \Lambda_{BB}(\phi_A,\phi_B)\left[\frac{1}{N_B\phi_B} + \frac{1}{\phi_V} + \chi_{BB} + \chi_{VV} - 2\chi_{BV}\right] \quad (20d)$$

Combining now eqs 19 and 20 with the continuity equation, eqs 8a and b, we obtain the desired set of two coupled diffusion equations describing interdiffusion

$$\frac{\partial\phi_A(\vec{r},t)}{\partial t} = \nabla\{D_{AA}(\phi_A,\phi_B)\nabla\phi_A\} + \nabla\{D_{AB}(\phi_A,\phi_B)\nabla\phi_B\} \quad (21a)$$

$$\frac{\partial\phi_B(\vec{r},t)}{\partial t} = \nabla\{D_{BA}(\phi_A,\phi_B)\nabla\phi_A\} + \nabla\{D_{BB}(\phi_A,\phi_B)\nabla\phi_B\} \quad (21b)$$

For the case where a layer of polymer A is brought on top of a layer of polymer B, which is the situation

considered in some of the experiments[17,18,26,27] and some theoretical treatments,[4,6] only concentration variations in the z direction perpendicular to the layers are of interest and hence ∇ in eq 21 means $\partial/\partial z$. Previous theories,[4,6] however, have only considered a single diffusion equation for the relative volume fraction ϕ of one species, where $D(\phi)$ is the interdiffusion coefficient

$$\frac{\partial \phi}{\partial t} = \frac{\partial}{\partial z}\left\{D(\phi)\frac{\partial \phi}{\partial z}\right\} \tag{22}$$

Although physically in polymer melts one is interested in small vacancy concentrations $\phi_V \ll 1$, the limiting case $\phi_V \to 0$ ("incompressible" polymer mixtures[1-4]) is very delicate. Although in this limit $\nabla\phi_A(\vec{r},t) = -\nabla\phi_B(\vec{r},t)$ due to eq 6, one must not use this relation in eq 21a or eq 21b in order to reduce them to eq 22: in fact, eqs 21a and b are mutually consistent for $\nabla\phi_A \equiv -\nabla\phi_B$, $\partial\phi_A/\partial t \equiv -\partial\phi_B/\partial t$ only if the condition postulated by Sillescu[7] would hold

$$\Lambda_{AA} = -\Lambda_{AB} = \Lambda_{BB} \tag{23}$$

Now eq 23 makes no sense for our lattice model, where two independent mobilities for the jumps of A monomers to a vacant lattice site and of B monomers to vacant lattice sites exist. In fact, the mistake made in this direct reduction of eq 21 to eq 22 is that the Onsager coefficients Λ_{AA}, Λ_{AB}, and Λ_{BB} are all proportional to ϕ_V in the limit $\phi_V \to 0$: So if we take this limit first before solving our differential equations, eq 23 is satisfied because all Onsager coefficients are zero!

Thus the proper procedure to solve the interdiffusion problem inevitably amounts to first solve the coupled set of diffusion equations, eqs 21a and b, for nonzero ϕ_V, even if one eventually wants to consider the limit $\phi_V \to 0$ in the final result. For the interpretation of the simulations presented in the next sections, where ϕ_V is not small, a fully general situation needs to be treated. Note that the Onsager formalism does not make any predictions on the concentration dependence of $\Lambda_{AA}(\phi_A,\phi_B)$, $\Lambda_{AB}(\phi_A,\phi_B)$, and $\Lambda_{BB}(\phi_A,\phi_B)$ for general volume fractions ϕ_A and ϕ_B: since eqs 21a and b involve due to eqs 20 also terms $\partial\Lambda_{AA}(\phi_A,\phi_B)/\partial\phi_A$, $\partial\Lambda_{AA}(\phi_A,\phi_B)/\partial\phi_B$, and so forth, any further progress with the description of the dynamics of nonlinear concentration variations, as they occur when the interface between layers of pure polymer A and pure polymer B broadens, is very difficult. A more microscopic theory is needed, which predicts the concentration dependences of the various Onsager coefficients involved in eqs 20 and 21. Since already the solution of eq 22 requires numerical work,[4,26,27] numerical methods are also required for solving eqs 21a and b, and a general explicit solution for unknown $\Lambda_{AA}(\phi_A,\phi_B)$, $\Lambda_{AB}(\phi_A,\phi_B)$, and $\Lambda_{BB}(\phi_A,\phi_B)$ cannot be written down.

Progress, however, can be made in the simpler situation where the concentration variations $\nabla\phi_A$ and $\nabla\phi_B$ are so small that one can linearize eqs 21a and b in these gradients and rather solve the set of equations

$$\frac{\partial \phi_A(\vec{r},t)}{\partial t} = D_{AA}(\phi_A,\phi_B)\nabla^2\phi_A(\vec{r},t) + D_{AB}(\phi_A,\phi_B)\nabla^2\phi_B(\vec{r},t) \tag{24a}$$

$$\frac{\partial \phi_B(\vec{r},t)}{\partial t} = D_{BA}(\phi_A,\phi_B)\nabla^2\phi_A(\vec{r},t) + D_{BA}(\phi_A,\phi_B)\nabla^2\phi_B(\vec{r},t) \tag{24b}$$

Equations 24a and b are meaningful, if one considers either the interdiffusion of layers, which differ only weakly in concentration (i.e., one layer has concentrations ϕ_A and ϕ_B; the other has $\phi_A + \delta\phi_A$ and $\phi_B + \delta\phi_B$, $\delta\phi_A \ll 1$ and $\delta\phi_B \ll 1$) or spontaneous concentration fluctuations in a macroscopically homogeneous material. The latter situation is relevant if the dynamics of concentration fluctuations is measured by coherent scattering of light, X-rays, or neutrons, including the behavior in the initial stages of spinodal decomposition.[1-3,10]

We now seek solutions of eqs 24a and b, which have the form of a concentration wave

$$\phi_A(\vec{r},t) = \phi_A^0 + \delta\phi_A^k e^{i\vec{k}\cdot\vec{r}} \exp(-Dk^2t) \tag{25a}$$

$$\phi_B(\vec{r},t) = \phi_B^0 + \delta\phi_B^k e^{i\vec{k}\cdot\vec{r}} \exp(-Dk^2t) \tag{25b}$$

$\vec{k}$ being the wavevector of the concentration wave, and D then is an effective interdiffusion constant. Equations 24a and b yield two solutions for D, which we call D_+ and D_-:

$$D_\pm = \frac{1}{2}\{D_{AA}(\phi_A^0,\phi_B^0) + D_{BB}(\phi_A^0,\phi_B^0)\} \pm \frac{1}{2}\{[D_{AA}(\phi_A^0,\phi_B^0) - D_{BB}(\phi_A^0,\phi_B^0)]^2 + 4D_{AB}(\phi_A^0,\phi_B^0)D_{BA}(\phi_A^0,\phi_B^0)\}^{1/2} \tag{26}$$

Thus the deviations $\partial\phi_A^k$ and $\delta\phi_B^k$ of the concentrations from their equilibrium values ϕ_A^0 and ϕ_B^0 decay with two decay constants, the smaller of which (D_-) dominates, of course, the decay at late times. From eq 26 one now can prove the comments made above about the limit $\phi_V \to 0$. For small ϕ_V we find (omitting again the superscripts zero from the equilibrium concentrations to simplify the notation), after some simple but tedious algebra

$$D_+ \approx (\Lambda_{AA} + 2\Lambda_{AB} + \Lambda_{BB})/\phi_V \tag{27a}$$

$$D_- \approx \frac{\Lambda_{AA}\Lambda_{BB} - \Lambda_{AB}^2}{\Lambda_{AA} + 2\Lambda_{AB} + \Lambda_{BB}}\left\{\frac{1}{N_A\phi_A} + \frac{1}{N_B\phi_B} + \chi_{AA} + \chi_{BB} - 2\chi_{AB}\right\} \tag{27b}$$

Since in this considered limit Λ_{AA}, Λ_{BB}, Λ_{AB}, are proportional to ϕ_V, it is clear that D_+ describes the "density relaxation" (i.e., the decay of fluctuations of the total volume fraction $\phi_A + \phi_B$ of both A and B monomers, balanced by a vacancy current; compare eqs 27a and 13c, while D_- describes interdiffusion. This diffusion coefficient for interdiffusion now has the familiar form of the product of a "kinetic factor" involving only the Onsager coefficients $\{(\Lambda_{AA}\Lambda_{BB} - \Lambda_{AB}^2)/(\Lambda_{AA} + 2\Lambda_{AB} + \Lambda_{BB})\}$ and a thermodynamic factor, which simply can be interpreted as $[\partial^2(f/k_BT)/\partial\phi_A^2]_T$, using the free energy expression, eq 7, and $\phi_V = 0$ and eliminating then ϕ_B with the help of eq 6 as $\phi_B = 1 - \phi_A$. In this limit $\phi_V \to 0$, it is clear that the interactions involving vacancies $\{\chi_{AV}, \chi_{BV}, \chi_{VV}\}$ must cancel out from D_+ and D_- and that the other interactions χ_{AA}, χ_{BB}, and χ_{AB} enter only in the familiar combinations χ defined above.

The simulation presented in the next sections involves a rather large volume fraction of vacancies ϕ_V, however, and also eq 7 with ϕ_V of order 10^{-2}–10^{-1} is a more realistic description of real polymer blends rather than the incompressible case, $\phi_V \to 0$. Therefore, we emphasize that for ϕ_V nonzero eqs 27a and b still hold as long as the

following inequalities hold simultaneously:

$$\left(\frac{1}{\phi_A N_A} + \chi_{AA} + \chi_{VV} - 2\chi_{AV}\right)\phi_V \ll 1 \quad (28a)$$

$$\left(\frac{1}{\phi_B N_B} + \chi_{BB} + \chi_{VV} - 2\chi_{BV}\right)\phi_V \ll 1 \quad (28b)$$

$$(\chi_{AB} + \chi_{VV} - \chi_{AV} - \chi_{BV})\phi_V \ll 1 \quad (28c)$$

For small molecules ($N_A = N_B = 1$) eqs 28a and b require $\phi_V \ll 1$, while for compatible polymer blends, for which all interaction parameters χ_{ij} are zero or very small eqs 28a–c remain true for rather large vacancy concentrations, namely

$$\phi_V \ll \phi_A N_A, \phi_V \ll \phi_B N_B \quad (29)$$

which for large chain lengths is always true, except for the case where one species becomes very dilute (e.g., at the tails of the concentration profile).

We now show that D_+ and D_- in the case where eqs 28a–c hold actually describe density relaxation and interdiffusion. While a general initial condition $\delta\phi_A^k$ and $\delta\phi_B^k$ in eqs 25a and b decays with time with both exponential factors $\exp(-D_+k^2t)$ and $\exp(-D_+k^2t)$, we construct now special initial conditions, which decay with either $\exp(-D_+k^2t)$ or $\exp(-D_-k^2t)$ only. From eq 24a, for instance, we thus find

$$\delta\phi_A^{k+}(-D_+ + D_{AA}) + \delta\phi_B^{k+}D_{AB} = 0 \quad (30a)$$

$$\delta\phi_A^{k-}(-D_- + D_{AA}) + \delta\phi_B^{k-}D_{AB} = 0 \quad (30b)$$

and by using eqs 20, 27, and 28, this can be reduced to

$$\delta\phi_B^{k-}/\delta\phi_A^{k-} = -1 + O(\phi_V) \quad (31a)$$

$$\delta\phi_B^{k+}/\delta\phi_A^{k+} = (\Lambda_{AB} + \Lambda_{BB})/(\Lambda_{AB} + \Lambda_{AA}) > 0 \quad (31b)$$

Thus choosing $\delta\phi_B^k$ and $\delta\phi_A^k$ of the same sign, such that there is a variation of the "density" $\phi_A(\vec{r}) + \phi_B(\vec{r})$, we obtain a mode relaxing with D_+. Only if we choose $\delta\phi_B^k$ and $\delta\phi_A^k$ of opposite sign and equal magnitude, eq 31a, we have a relaxation involving D_- only. But this is exactly the situation of interdiffusion, where there is no density variation in the system but a variation of relative concentration of the species A and B.

We now discuss eq 27b and make the following two approximations, in order to make contact with the so-called "slow mode theory", eq 1.

(i) We neglect the off-diagonal Onsager coefficient, Λ_{AB}, in comparison with the diagonal ones; i.e., we postulate

$$\Lambda_{AB} \ll \Lambda_{AA}, \quad \Lambda_{AB} \ll \Lambda_{BB} \quad (32)$$

Although this approximation has been made implicitly in most previous work,[3,4,6,10,12] there is not really any physical justification for it: And, in fact, recent simulations for the noninteracting simple lattice gas[15] show that in this model eq 32 is not true.

(ii) We expand the diagonal Onsager coefficients, Λ_{AA} and Λ_{BB}, in leading order in volume fractions ϕ_V, ϕ_A, and ϕ_B as

$$\Lambda_{AA} = \phi_V\phi_A\lambda_A, \quad \Lambda_{BB} = \phi_V\phi_B\lambda_B \quad (33)$$

where λ_A stays nonzero and finite as $\phi_A \to 0$ and λ_B stays nonzero and finite as $\phi_B \to 0$. In these limits, eq 27b yields, using eq 32

$$D_-(\phi_A \to 0) = \phi_V\lambda_A/N_A, \quad D_-(\phi_B \to 0) = \phi_V\lambda_B/N_B \quad (34)$$

Since $D_-(\phi_A \to 0) = D_A^*$, the tracer diffusion coefficient of an A chain in a B matrix, and $D_-(\phi_B \to 0) = D_B^*$, the tracer diffusion coefficient of a B chain in an A matrix, we can rewrite eq 33 with the help of eq 34 as follows:

$$\Lambda_{AA} = \phi_A N_A D_A^*, \quad \Lambda_{BB} = \phi_B N_B D_B^* \quad (35)$$

For $\chi = 0$ eq 27b then is reduced to eq 1, since for $\Lambda_{AB} = 0$ the "kinetic factor" in eq 27b is just $(\Lambda_{AA}^{-1} + \Lambda_{BB}^{-1}) = [N_A D_A^*\phi_A)^{-1} + (N_B D_B^*\phi_B)^{-1}]^{-1}$. Now while $\Lambda_{AA} = \phi_V\phi_A/\lambda_A$ must be true for $\phi_A \to 0$ in order that $D_-(\phi_A \to 0)$ tends to a finite nonzero limit, then is no reason to assume λ_B to be independent of ϕ_A and ϕ_B either. Thus eq 1 is not a general consequence of the vacancy model of polymer diffusion but only results if the two further approximation eqs 32 and 33 are made. Similarly, the fast mode theory, eq 2, results from eqs 8 and 14 if we also invoke eq 32, neglecting nondiagonal terms in eqs 14a and b, and furthermore postulate[6]

$$\nabla\mu_V = 0 \quad (36)$$

While a real polymer mixture is a fluid where density gradients may relax via hydrodynamic flows and eq 36 may be a much more reasonable assumption rather than insisting on a rigid ideal lattice and its consequences, a justification of eq 32 in this case also seems questionable and remains to be given. Another problem, which we consider as completely unsolved, is the question of whether it would be a reasonable approximation to replace the nonlinear problem, eq 21, by eq 22 and interpreting $D(\phi)$ as the interdiffusion coefficient $D_-(\phi)$ there: in our opinion, this is implicitly assumed by Brochard et al.[4] and others,[26,27] where eq 22 is solved by using eq 27b. Using eqs 32 and 35 in eqs 20 and 21, one could attempt to find numerical solutions of the latter, but this problem is left to future publication. Thus, even in the framework of simple model assumptions, the phenomenological theory of interdiffusion is far from being fully understood.

3. Model and Simulation Technique

While the static properties of lattice models for polymer blends have been studied with Monte Carlo techniques extensively in recent years,[35–37] dynamical properties have found much less attention. The initial stages of spinodal decomposition in a two-dimensional polymer blend with strong nearest-neighbor interactions was simulated[38] with the "slithering-snake"[39,40] algorithm: of course, this algorithm is not at all microscopically realistic. We apply an algorithm that is realistic in the sense that for isolated chains on lattices it yields a dynamics consistent with the Rouse model,[41] and it should have not too severe ergodicity problems even for relatively dense systems.[42] A newly developed "bond length fluctuation" algorithm prepared by two of us[43] satisfies these criteria at all dimensions (the algorithm of refs 35–37 would not be useful for two-dimensional lattices, of course[42]).

We consider a square lattice ($d = 2$) or a simple cubic lattice ($d = 3$) and put the lattice spacing equal to unity. Each monomer occupies four ($d = 2$) or eight ($d = 3$) lattice sites of a unit cell. Each lattice site can either be empty or be part of one monomer only: thus local excluded-volume constraints are satisfied. Each polymer consists now of N monomers connected by bonds whose lengths are not fixed but restricted in bond length l to be smaller than 4. To move the chain, a monomer is selected at random. Then it tries, at random, to jump the distance of one lattice unit into one of the 2 times d lattice directions. If the move complies with both the bond length restriction and the excluded-volume condition, it is carried out (Figure 1a); otherwise, it is rejected and a new monomer

Table I
Tracer Diffusion Constant Times N, $6DN$ for Different Concentrations and Chain Lengths[a]

	diffusion constants $6DN$					
	lattice gas		$N = 10$		$N = 20$	
	25%	50%	25%	50%	25%	50%
1 in 1	0.5	0.19	0.25	0.076	0.22	0.071
1 in 2	0.55	0.23	0.30	0.10	0.28	0.094
2 in 1	0.88	0.30	0.39	0.11	0.39	0.096
1 in 10	0.65	0.28	0.35	0.17	0.36	0.157
10 in 1	2.94	0.67	1.14	0.22	0.92	0.23

[a] For details see text. Here always the diffusion of a single chain/lattice gas particle in the matrix of the host of the density indicated is measured.

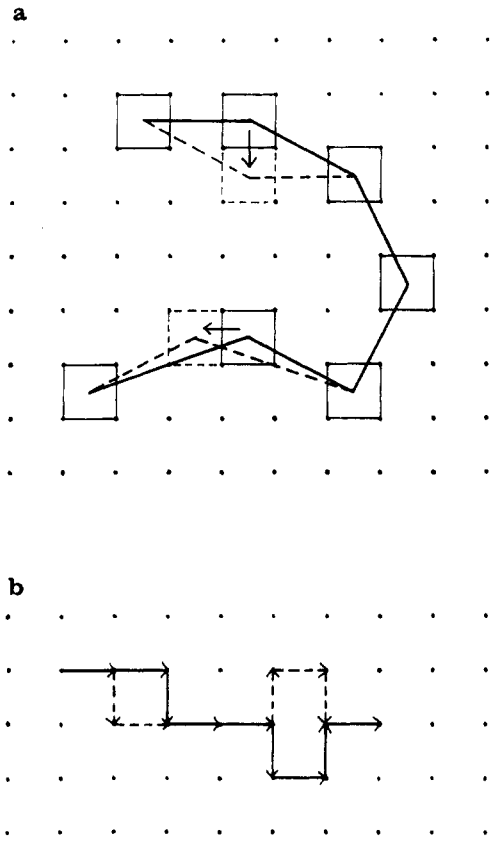

Figure 1. Two-dimensional illustration of the bond length fluctuation algorithm (upper part) compared to the standard algorithm (lower part) on the square lattice. Full lines indicate the original configuration, while the broken lines indicate possible new configurations. For the standard kink-jump method (lower part) bond vectors are indicated by arrows in order to point out the "bond exchange" in the course of the kink-jump moves.

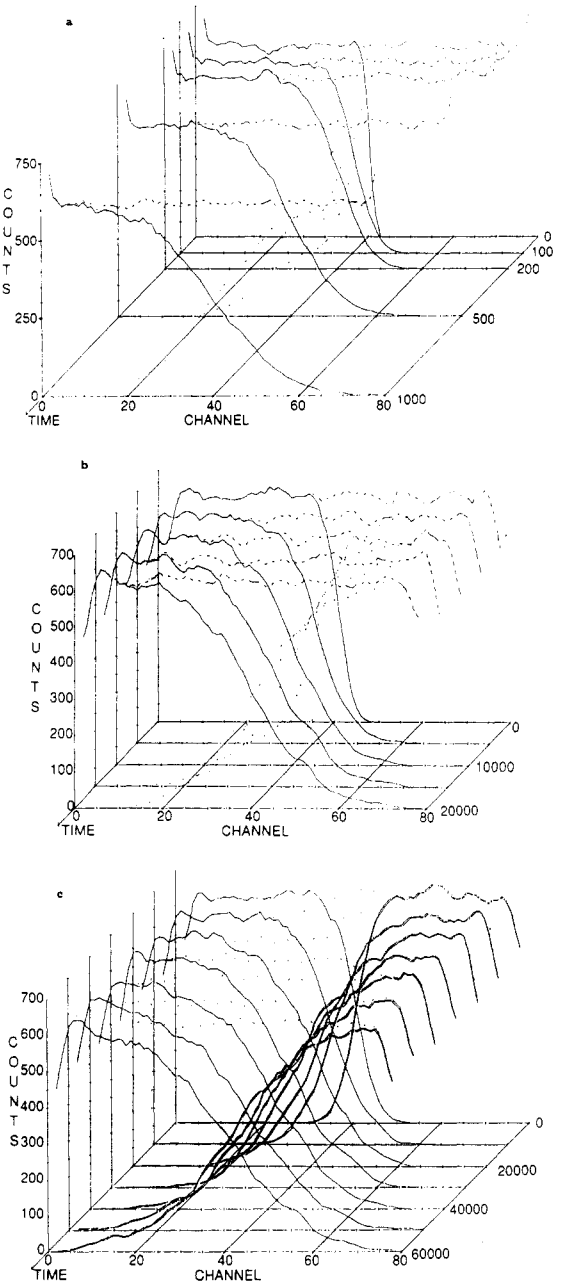

Figure 2. Concentration profiles $\phi_A(z,t)$, $\phi_B(z,t)$, and $c(z,t) = \phi_A(z,t) + \phi_B(z,t)$ plotted for several times t for $N = 1$ (a), $N > 10$ (b), and $N = 20$ (c). Parameters chosen are $v = 1$ and $c = 0.25$. Note that the concentration is not normalized to unity in this and the following figures, but rather the "count" of occupied sites in each "channel" (i.e., lattice plane at coordinate z, summed over all 48 systems simulated) is shown.

is selected at random, and so on. The elementary time unit is Γ_i attempted moves per monomer of the system, where Λ_i is the relative mobility of the species i (i = A and B). In this algorithm, bond vectors and lengths within a polymer are not conserved, in contrast to standard algorithms (Figure 1b).

We choose a system of size $20 \times 20 \times 80$ (only three-dimensional studies will be presented here), applying periodic boundary conditions in the x and y directions, while we use a hard-wall boundary condition at $z = 0$ and $z = 81$. The z direction is the direction in which the interdiffusion takes place; thus, this linear dimension has to be larger than the other two. The simulations were performed on the Siemens-Fujitsu VP100 vector computer of the University of Kaiserslautern. In order to make efficient use of the vector performance of the computer, always 48 independent systems were simulated in parallel. Averaging the results of these 48 systems, we get a reasonable statistical accuracy of the concentration profiles we obtained.

Three different chain lengths, N (N = 1, 10, and 20), and two different ϕ ($\phi = \phi_A + \phi_B = 0.25$ and 0.50) have been studied. The two species were only allowed to differ in their mobilities Γ_A and Γ_B, respectively. We investigated three mobility ratios Γ_A/Γ_B = 1, 0.5, and 0.1.

As a first step in the simulation we have to generate an equilibrated homogeneous melt of only one species. This has been achieved by continuously growing the chains up to the desired chain length, N. During the growth procedure the already existing parts of the chains move around by using the algorithm as explained above. After generating the preliminary 48 configurations, we ran the systems several diffusion times of the chains. This ensures

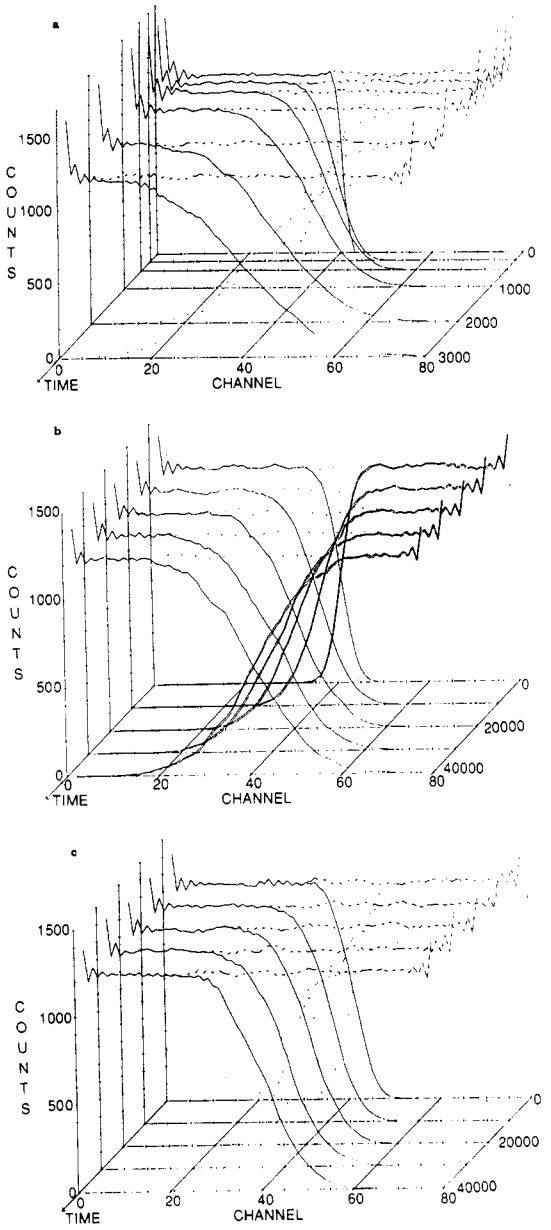

Figure 3. Same as Figure 2 but for $c = 0.50$.

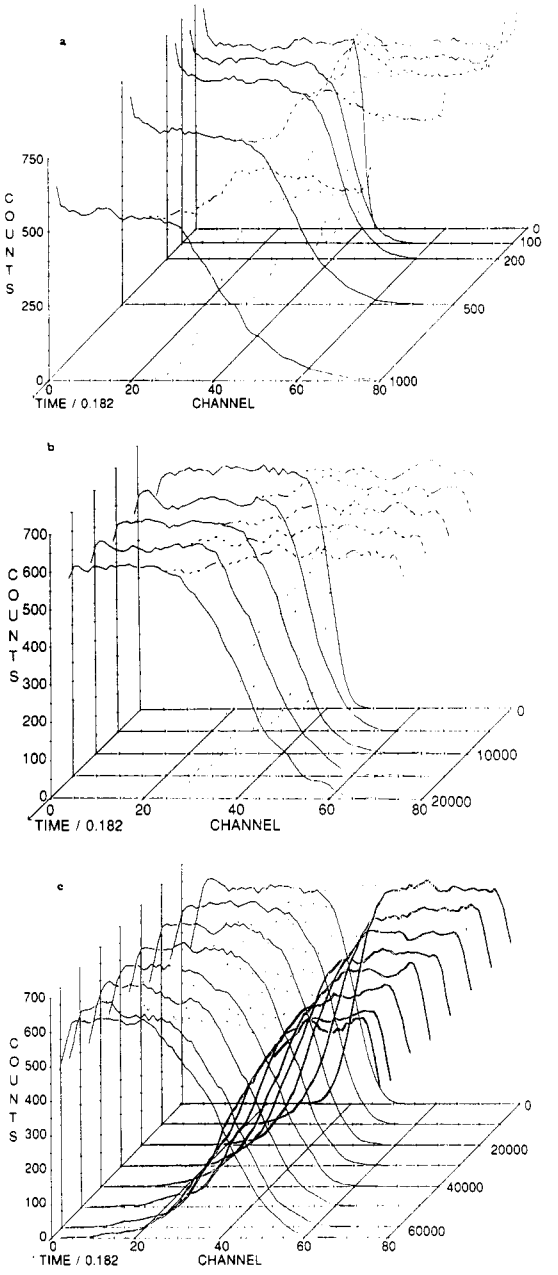

Figure 4. Same as Figure 2 but for $v = 10$.

that the relaxed initial configuration then used for the sampling was equilibrated. The diffusion times can be taken from Table I. The time unit, τ, then is given by one attempted move for each monomer of the whole system. As one can see from these data for $c = 0.25$, the relaxation times are more than a factor of two smaller than for the $c = 0.50$ case. However, the acceptance rate, δ, of the attempted moves roughly varies linearly within the concentrations considered here ($N = 1$; $c = 0.50$, $\delta \approx 0.70$; $c = 0.25$, $\delta = 0.36$; $N = 10$; $c = 0.50$, $\delta = 0.24$; $c = 0.25$, $\delta = 0.45$). This discrepancy means, that the model develops backjump correlations, as expected to occur in such collective systems, even for the monomer case. For the models of refs 15 and 35–37 this is more unlikely since the monomers may move several lattice constants during one move.

When the system is well equilibrated, one stores 48 distinct configurations (which are far enough away in time to be essentially statistically independent of each other), which are used as the initial configurations for the interdiffusion simulations. While so far all chains (or monomers, respectively) have been treated as identical, one now calls all chains with centers of gravity in the left half of the system ($z \leq 40$) A chains, and chains with centers of gravity in the right half ($40 < z \leq 80$) B chains. In this way, the relative monomer concentration $2\phi_A/(\phi_A + \phi_B)$ changes from unity for small z to zero at large z, with an initially rather sharp interface at $z = 40$. Of course, the initial monomer profile created in this way is not a step function, but it has width that is of the order of the gyration radius $\langle R_{gyr}^2 \rangle^{1/2}$. For Gaussian chains, we expect $\langle R_{gyr}^2 \rangle \approx l^2 N/6$, which would imply that the initial width is of the order of 5–8 lattice spacings. (Only in the monomeric case $N = 1$ occurs a rather sharp interface extending over two lattices planes only, since each monomer occupies sites in two adjacent lattice planes. In order to reduce the scatter of the density profile data, the density values were averaged over 5 "channels", where the channel count with a factor 4, 2, and 1 from the center. While this artificially broadens the profile for the $N = 1$ case, the effect is rather insignificant for the polymer case.) Since the estimation of the interdiffusion constant from the spreading of the interfacial profile requires the study of interfacial widths, which are much larger than the initial width but much smaller than the total linear dimension

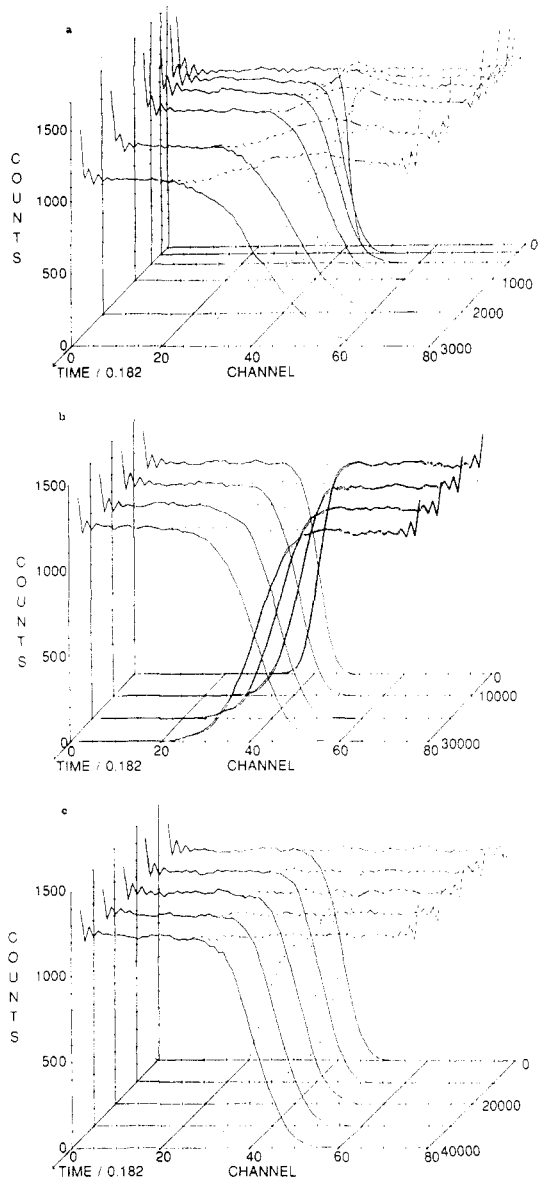

Figure 5. Same as Figure 2 but for $v = 10$ and $c = 0.50$.

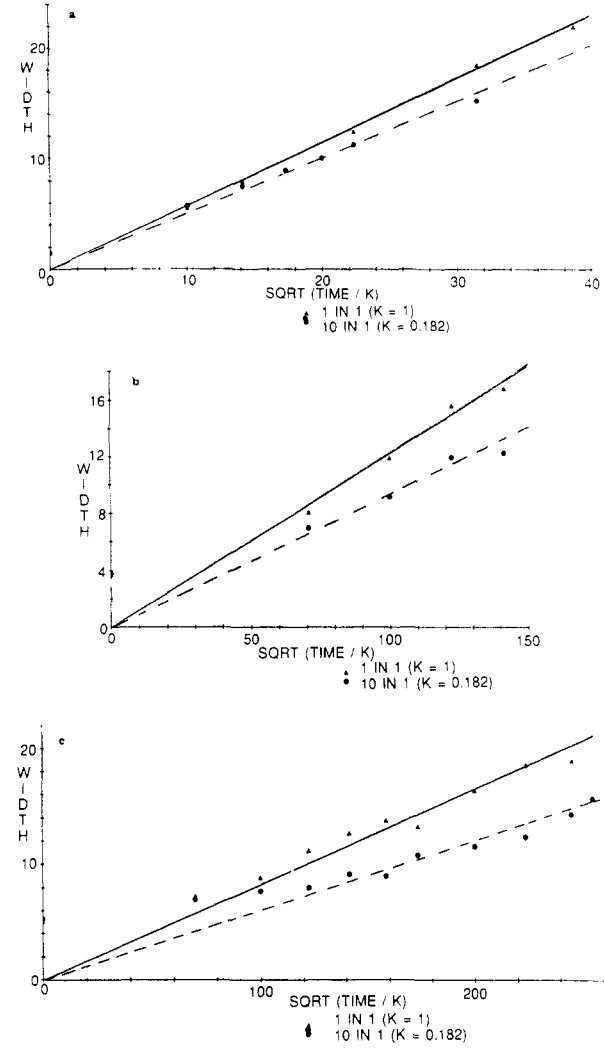

Figure 6. Interquartile width $W_{1/2}$ plotted versus the square root of time for the monomer case (a), $N = 10$ (b), and $N = 20$ (c). All data refer to a concentration $c = 0.25$. The three mobility ratios $v = 1$, 2, and 10 are represented by different symbols, as indicated in the figure.

L_z in the z direction, it is clear that we had to choose an L_z as large as $L_z = 80$, while in the other directions it is only necessary to choose linear dimensions distinctly exceeding $(\langle R_{gyr}^2 \rangle)^{1/2}$. Note also that the position of the interface is fixed at $z = 40$ only initially, but as time develops the interface position is free to move: due to the strict conservation of both monomers and vacancies in our model and the use of a rigid lattice, this motion would of course involve the buildup of a density gradient. As will be seen below, this actually happens for the monomer case where Γ_A differs strongly from Γ_B but hardly occurs for long polymer chains.

We conclude this section with some comments on the estimation of self-diffusion coefficients. There we rely only on the Einstein relation (α = A or B)

$$D_\alpha^* = \langle [\vec{r}_i^{\,\alpha}(t + t_0) - \vec{r}_i^{\,\alpha}(t_0)]^2 \rangle / 6t, \quad t \to \infty \qquad (37)$$

where $\vec{r}_i^{\,\alpha}(t)$ is the position of the center of gravity of a chain (labeled by index i) of type α at time t. Note that the thermal equilibrium D_α^* should be independent of the time t_0, used as the origin of time for the calculation of the mean-square displacement in eq 37. When we use eq 37 for the motion of chains in our finite geometry, care has to be taken to avoid spurious finite size effects: first, only such chains are considered whose centers of gravity are far enough from the hard walls, such that during the time interval considered no monomer of the chains has a chance to come in contact with the wall. Second, in the directions where the periodic boundary conditions are used in the Monte Carlo generation of the configurations of the chains, we use a second set of coordinates for the calculation of the mean-square displacement; this second set of coordinates precisely has the effect of undoing the periodic "images" of the basic simulated finite cell. Third, with interest in D_α^* when component α is dilute ($\phi_\alpha \to 0$) it is important to look at as many chains as possible in order to obtain good statistics. In practice, we hence typically follow the mean-square displacement of four chains, whose centers of gravity are selected from the intervals, $15 \le z \le 17$, $30 \le z \le 32$, $45 \le z \le 47$, and $60 \le z \le 62$, respectively: during the time interval considered, these four chains then can neither overlap nor reach the solid walls. Of course, this problem only arises for $\Gamma_A \neq \Gamma_B$, while for $\Gamma_A = \Gamma_B$ every chain can be labeled and used for eq 37, provided its center of gravity is in the interval $15 \le z \le 62$.

Finally we recall that the choice of the time unit within Monte Carlo dynamics is completely arbitrary; besides that, this unit has to vary linearly with the number of particles in the whole system.[42-46] We measure time in units of attempted moves per monomer of the slow component.

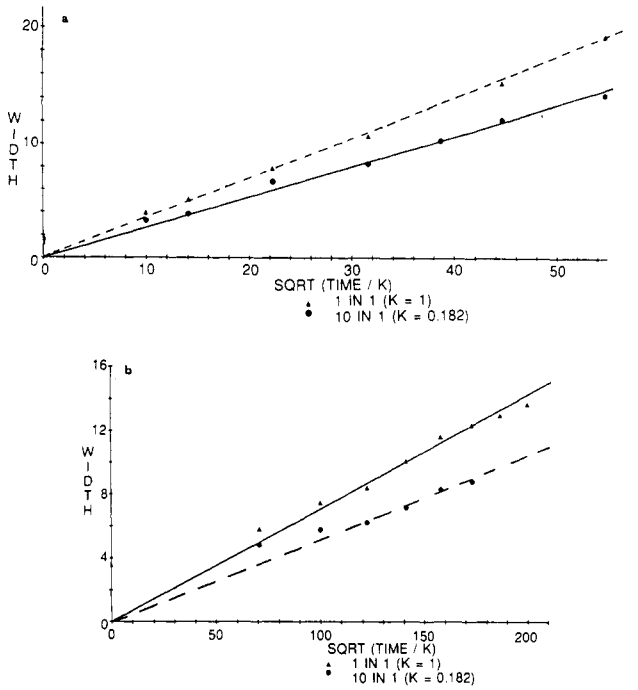

Figure 7. Same as Figure 6 but for $c = 0.50$, but only for $N = 1$ (a) and $N = 10$ (b).

4. Monte Carlo Simulation Results for the Interfacial Broadening

The "raw data" of the simulations for a ratio $v \equiv \Gamma_A/\Gamma_B = 1$ and a polymer concentration $c = \phi_A + \phi_B = 0.25$ and $c = 0.50$ are shown in Figures 2 and 3. While for $c = 0.25$ rather strong density fluctuations occur; these density fluctuations are already strongly suppressed for $c = 0.50$. We hence feel that $c = 0.50$ already corresponds to an incompressible polymer melt, while $c = 0.25$ still may physically correspond to a (concentrated) polymer solution. Note that one should not consider the maximum value of packing $c = 1$ as relevant for a polymer melt; $c = 1$ can only be realized in a perfectly frozen state, where no motion whatsoever is possible in our model; it rather corresponds to a polymer glass (or crystal, if the chains are regulary placed) at $T = 0$.

One further notices a very distinct effect of the wall for the two values of c studied. The monomer concentration near the wall is enhanced, while the polymer concentration for $c = 0.25$ is depressed. Since we do not have any finite interaction energies between monomers and the wall, these effects are of purely entropic origin. In no case, however, has this wall effect much structure, while for $c = 0.5$ distinct oscillations are seen, which decay after about 6 layers off the walls, and both in the monomer case and in the polymer case the concentration in the layer adjacent to the wall is enhanced. These interesting wall effects are outside the scope of the present investigations, however, and will be analyzed in a future study.

When we compare the profiles for the monomer (lattice gas) case $N = 1$ and the profiles for the polymers with chain lengths $N = 10$ and $N = 20$, systematic differences in the case $v = 1$ are not seen. Of course, the time scale for the broadening of the interface in the polymer case increases with increasing chain length N, consistent with the decrease in the self-diffusion constant of the chains, $D^* \propto N^{-1}$ in the Rouse regime, which is verified below. Brochard et al.[4] have predicted that for $t = \infty$ the concentration profiles asymptotically obtain a nonanalytic shape. If such a behavior actually occurs for our model, it can happen at time scales that only are much larger than those accessible in our simulation.

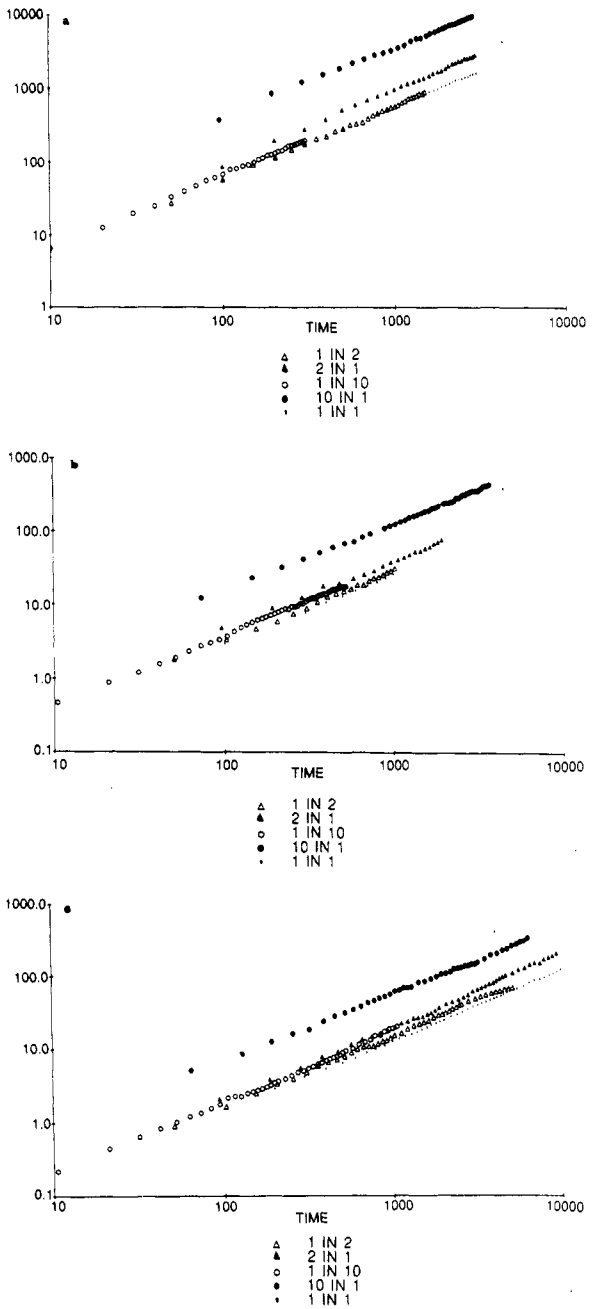

Figure 8. Mean-square displacement of a labeled chain plotted versus time, for $N = 1$ (a), $N = 10$ (b), and $N = 20$ (c). All data refer to $c = 0.25$. Different symbols represent different choices of the mobility ratio v, as indicated in the figure.

Figures 4 and 5 show the similar data for $v = 10$. It is seen that the lattice gas results now display a behavior very different from that seen for $v = 1$: at the part of the interfacial profile where initially the slow monomers are, the concentration $c(z,t)$ always is distinctly enhanced, while it is decreased on the other side. The region where this enhancement occurs broadens with increasing time, just as the interfacial profile itself. The physical interpretation of this phenomenon, of course, is clear: the fast species diffuses into the region taken by the slow species, and since there are enough vacancies present in the system, the motion of the fast species does not require the slow species to move away; the two concentration profiles $\phi_A(z,t)$ and $\phi_B(z,t)$ can broaden at somewhat different rates. In a real fluid, however, the buildup of such a density gradient as seen in Figures 4a and 5a would relax by a flow of the average interface position to the left, which cannot occur in our rigid lattice model.

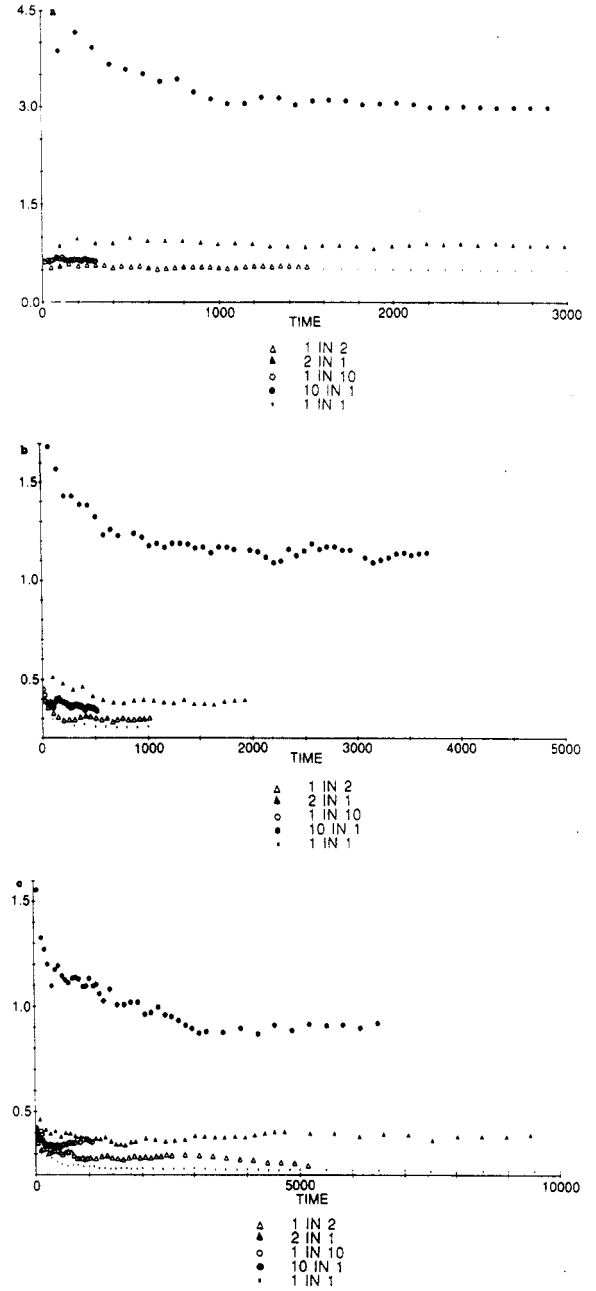

Figure 9. Same data as in Figure 8 but divided by the time, for $N = 1$ (a), $N = 10$ (b), and $N = 20$ (c).

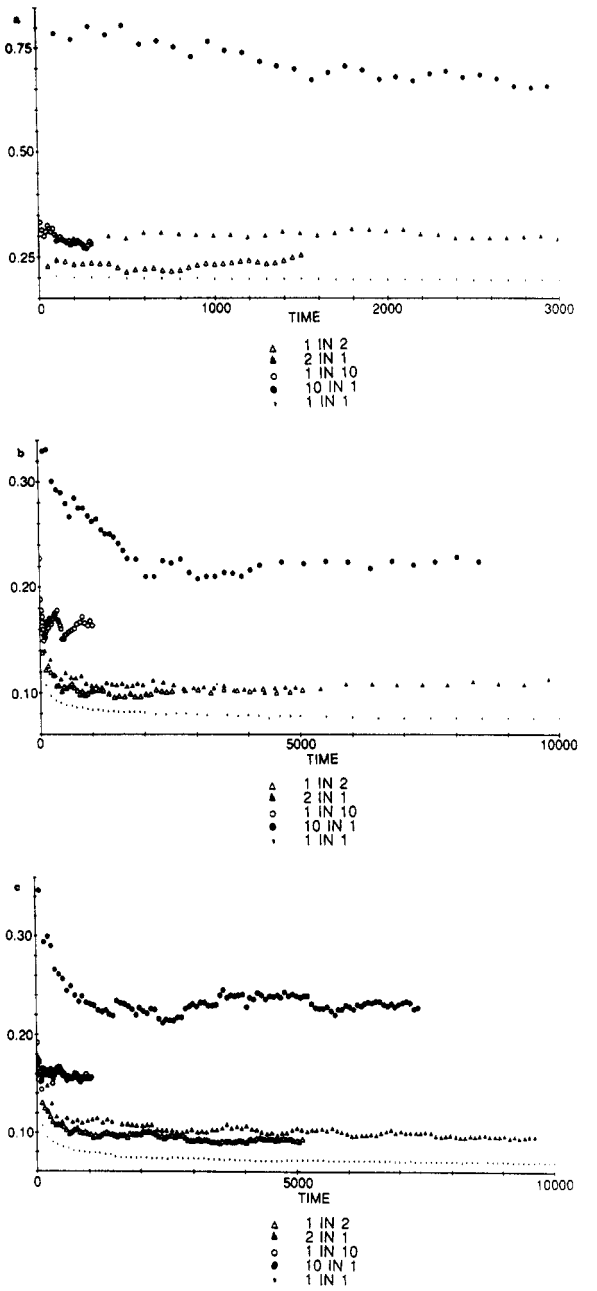

Figure 10. Same as Figure 9 but for $c = 0.50$.

While for $c = 0.25$ a mild precursor of this phenomenon seems to occur at least for short chains (Figure 4b; $N = 10$), for $c = 0.50$ in the polymer case it is clearly absent. This reiterates our conclusion that $c = 0.50$ already corresponds to an incompressible polymer mixture, and eq 29 for $c = 0.50$ in fact is satisfied for both chain lengths $N = 10$ and $N = 20$, while it clearly is not satisfied in the monomer case. The general shape of the broadening profiles in the polymer case is not qualitatively different from the profiles occurring for $v = 1$; the only distinction is a pronounced slowing down of the interdiffusion for $v = 10$, which prevented us from observing a strong broadening of the profiles, which would have needed a very large amount of computing time.

Results similar to the data shown above have also been obtained for $v = 2$. We also note the great similarity of our simulation results to the broadening of concentration profiles observed in corresponding real experiments.[26] This suggests also that an analysis of the simulated profiles along similar lines as performed in the experiments would be interesting. As in ref 26, we hence focus attention on the time evolution of the interquartile widths of the profiles. If eq 22 would hold and $D(\phi)$ in this equation would be independent of ϕ, the analytic solution to our problem is well-known[33] and the result for the time evolution of the interquartile width is ($W_{1/2}$ is the width of the profile between the concentration points $\phi_A/c = {}^1/_4$ and $\phi_A/c = {}^3/_4$)

$$W_{1/2}/\sqrt{t} = 2BD^{1/2} \tag{38}$$

with a coefficient $B = 1.10$.[33] For $D(\phi)$ in eq 22 not independent of ϕ we can also work with eq 38, interpreting D as $D(\phi_A{=}c/2)$, but B thus is slightly different.[4,6] The simulations are certainly consistent with a $t^{1/2}$ time dependence of the width $W_{1/2}$ (Figures 6 and 7); of course, fitting eq 38 to our data we can only determine the product of both parameters B and $D^{1/2}$, rather than both parameters separately. We shall return to this problem in section 6.

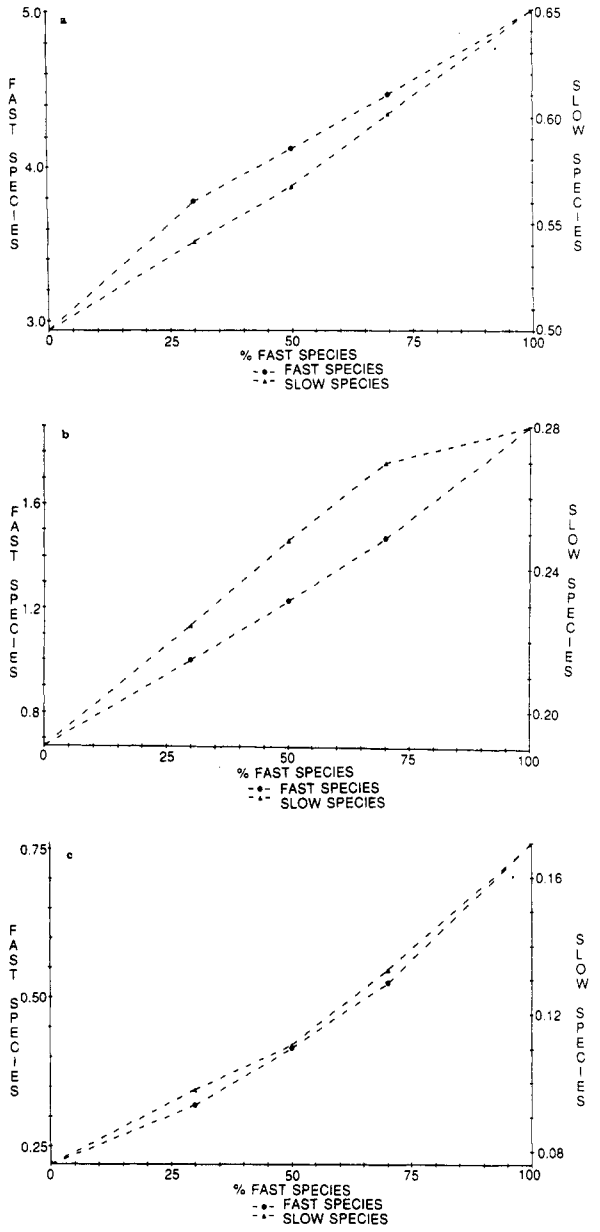

Figure 11. Diffusion constants ($6D = r^2(t)/t$) for three examples of fast and slow species as a function of composition for $v = 10$ for the lattice gas ((a) $c = 0.25$, (b) $c = 0.50$) and $6DN$ for short chains ($N = 10$) (c) for $c = 0.50$.

5. Simulation of Self-Diffusion in Polymer Blends

Typical results for the mean-square displacement of a labeled chain or a labeled monomer are shown in Figure 8. The results are consistent with a straight line behavior on the log–log plot, at least for large time, and hence eq 37 can be applied to extract D_α^* for the different cases. However, one has to be careful in not including too early times in a fit of the simulation results to eq 37, because deviations from eq 37 due to time-correlation effects[33,45] lead then to a systematic error. Therefore, it is advisable to rather plot the mean-square displacement divided by time, as written in eq 37, as a function of time, to observe over which regime of times eq 37 actually is valid (Figures 9 and 10). In the monomer case we see that time correlation effects only matter over a large time scale if the environment is much slower than the considered chain: if the jump rate of the considered chain is 10 times faster, the asymptotic regime obviously is only reached for $t \geq 10^3$ Monte Carlo steps of the slow chains. In the polymer case, however, there is always an initial regime where $\langle r^2 \rangle / t$ decreases. We interpret this finding as a consequence of the large size of the polymer coils.

The fact that much larger time scales must be passed for the case of a very slow environment of a monomer (or a polymer coil, respectively) implies, of course, that there the length scale over which the center of gravity must move is rather large, in order that purely diffusive behavior is observed. We interpret this phenomenon as a crossover effect toward anomalous diffusion, occurring exactly at the percolation threshold in a frozen-in environment.[47] At this percolation threshold, eq 37 does not hold, but one rather has $\langle r^2 \rangle \propto t^x$ with an exponent $x < 1$, which would imply in a plot like Figures 9 and 10 that $\langle r^2 \rangle / t$ is a monotonously decreasing function of time, which goes to zero as $t \to \infty$. To illustrate the effect of the surrounding more clearly, Figure 11 gives the chain (lattice gas) diffusion constants as a function of concentration of the fast species. These examples show the dramatic effect of the relative concentration on D as expected from the previous discussion. To discuss consequences of these results on the present problem of interdiffusion is an important future project. While for the ordinary lattice gas problem on the simple cubic lattice (where the size of the monomer is just a lattice site) the percolation concentrations is $c_p \simeq 0.31$,[47] we are not aware of any work estimating c_p for our generalized lattice gas with larger monomers.

A further analysis of this anomalous diffusion near the percolation threshold of the present model is beyond the scope of the present work. With respect to interdiffusion, we expect a drastic effect due to percolation if the slow species is concentrated enough such that the remaining volume is close to the percolation threshold. This phenomenon also has not yet been investigated.

From the horizontal parts of Figures 9 and 10 we have obtained via least-square fits the self-diffusion constants listed in Table I. Note that the polymer data are nicely consistent with the dependence on chain length N predicted by the Rouse model, $D_\alpha^* \propto N^{-1}$. These diffusion constants can now be used to evaluate the predictions of the slow and fast mode theories, eqs 3 and 4, and can be compared to our direct results on interdiffusion from the simulated interquartile widths. This will be done in the following section.

6. Discussion: Can the "Slow Mode Theory" or the "Fast Mode Theory" Account for the Simulation Results?

Let us ignore at this point the problem that the theory described in section 2 really would require us to deal with two coupled diffusion equations (eqs 21a and b) rather than with a single one (eq 22). We now assume eq 22 as a phenomenological description and invoke eqs 3 and 4 together with eq 38. This is exactly the procedure taken in the corresponding experimental work.[26]

Equations 3 and 4 have been proposed in the limit $\phi_V \to 0$, and there is the question of how one interprets these equations for finite fraction ϕ_V of vacancies. From the requirement that $D_{int} \to D_A^*$ of $\phi_A \to 0$ we conclude that ϕ_A and ϕ_B in eqs 3 and 4 then should be replaced by the relative volume fractions $\tilde{\phi}_A = \phi_A/(\phi_A + \phi_B) = \phi_A/(1 - \phi_V)$ and $\tilde{\phi}_B = \phi_B/(\phi_A + \phi_B) = \phi_B/(1 - \phi)$. Since $D(\phi = {}^1/_2)$ is required in eq 38, we hence obtain

$$W_{1/2}/\sqrt{t} = \beta\sqrt{2}(D_A^* + D_B^*)^{1/2}, \quad \text{fast mode theory} \quad (39a)$$

Table II
β-Values for the Interquartile Width for the Fast Mode (f) and the Slow Mode (s) Theory as a Function of the Determination of D^*[a]

		β-values									
		lattice gas				$N = 10$					
		25%		50%		25%		50%		$N = 20$: 25%	
		f	s	f	s	f	s	f	s	f	s
1/1		1.0		0.97		0.95		0.99		0.98	
10/1	A	1.07	1.39	1.1	1.2	0.97	1.14	1.07	1.08	0.95	1.05
	B	0.95	1.43	0.87	1.2	0.81	1.16	0.85	1.07	0.79	1.08
	C	0.86	1.51	0.74	1.28	0.71	1.24	0.73	1.27	0.69	1.19

[a] A: $D_A^* = D_A^*(1\rightarrow10); D_B^* = D_B^*(10\rightarrow1)$. B: $D_A^* = [D_A^*(1\rightarrow10) + D_A^*(1\rightarrow1)]/2; D_B^* = [D_B^*(10\rightarrow1) + D_B^*(10\rightarrow10)]/2$. C: $D_A^* = D_A^*(1\rightarrow1); D_B^* = D_B^*(10\rightarrow10)$. For mobility ratios and densities as indicated.

$$W_{1/2}/\sqrt{t} = \beta(2\sqrt{2})[D_A^* D_B^*/(D_A^* + D_B^*)]^{1/2}, \quad \text{slow mode theory} \quad (39b)$$

Of course, if $D_A^* = D_B^*$, both expressions coincide; thus, we can use the case $\upsilon = 1$ where $D_A^* = D_B^*$ holds to extract β from a fit of eq 39 to our interquartile widths. We find from this procedure values of β in the range $0.95 \leq \beta \leq 1.0$ (Table II), not very far from the value $\beta_0 = 1.10$ valid for a concentration-independent interdiffusion constant.[33] While Jordan et al.[26] always found values of β slightly exceeding 1.10, we find here somewhat smaller values. This may be a consequence of the fact that due to occupancy correlation effects the effective concentrations ϕ_A and ϕ_B that should be used in eqs 3 and 4 are not simply $\tilde{\phi}_A$ and $\tilde{\phi}_B$ as defined above but should be somewhat smaller. In any case, these effective concentrations should not depend on the ratio υ of jump rates. Thus a sensible test of eqs 39a and b is to require that for $D_A^* \neq D_B^*$ the same effective value of β should result as for $D_A^* = D_B^*$. Table II shows, however, that neither the fast mode theory nor the slow mode theory work very well.

We have also included alternative expressions in Table II where instead of the diffusion constants D_A^* and D_B^* suggested by theory (namely, the tracer diffusion coefficient of an A chain diluted in a B matrix and the tracer diffusion coefficient of a B chain diluted in an A matrix), which often are not easily accessible experimentally, we use the experimentally easier accessible tracer diffusion constants $D_A^*(A)$ and $D_B^*(B)$ of A(B) chains in the matrix of the same species. We see that with this choice, which has even less theoretical foundation, the agreement is even worse.

One source of discrepancies, of course, is the fact that the tracer coefficients D_A^* and D_B^* to be used in eqs 39a and b are themselves concentration dependent. Since we feel for the broadening of the interfacial profiles it may be most relevant to use the tracer diffusion constants for $\tilde{\phi} = {}^1/_2$, we approximate $D_A^*(\tilde{\phi} = {}^1/_2)$ by linear interpolation between $D_A^*(\tilde{\phi} = 0)$ and $D_A^*(\tilde{\phi} = 1)$, and similarly for D_B^*. Table II shows that also then quantitative agreement with the correct factor β is still not obtained.

Of course, there are several theoretical reasons why we expect neither eq 39a nor eq 39b to be quantitatively reliable: (i) Nondiagonal Onsager coefficients Λ_{AB} matter. (ii) Equations 27a and b hold only for small concentration deviations from the average concentration; for the strong concentration variations studied here ($\tilde{\phi}$ varies from 0 to 1 through the profile) the solution of the full nonlinear problem, eqs 21a and b, must be sought. (iii) One must pay attention to the proper concentration dependences of both Onsager coefficients and self-diffusion coefficients, as done for the simple lattice gas problem,[15] to check the theory fully.

In view of all these problems, we feel that the conclusion of experimental work, where sometimes it was concluded that the slow mode theory works and sometimes that the fast mode theory works, perhaps are overly optimistic. We rather expect that a close examination of the data will also reveal quantitative problems. Note that in our case, where a variation of Γ_A/Γ_B over 1 decade was allowed for, both the slow mode theory and the fast mode theory still yield roughly the correct order of magnitude; the error in the value of D_{int} usually is less than a factor of 2. Thus rather precise measurements are needed to significantly check the theories.

References and Notes

(1) de Gennes, P.-G. *J. Chem. Phys.* **1980**, *72*, 4756.
(2) Pincus, P. *J. Chem. Phys.* **1981**, *75*, 1996.
(3) Binder, K. *J. Chem. Phys.* **1983**, *79*, 6387.
(4) Brochard, F.; Jouffroy, J.; Levinson, P. *Macromolecules* **1983**, *16*, 1638.
(5) Brochard, F.; Jouffroy, J.; Levinson, P. *J. Phys. Lett.* **1983**, *44*, L-455.
(6) Kramer, E. J.; Green, P.; Palmstrom, C. *Polymer* **1984**, *25*, 473.
(7) Sillescu, H. *Makromol. Chem., Rapid Commun.* **1984**, *5*, 519.
(8) Brochard, F.; de Gennes, P.-G. *Europhys. Lett.* **1986**, *1*, 221.
(9) Akcasu, A. Z.; Benmouna, M.; Benoit, H. *Polymer* **1986**, *27*, 1935.
(10) Binder, K. *Colloid Polym. Sci.* **1987**, *265*, 273.
(11) Sillescu, H. *Macromol. Chem., Rapid Commun.* **1987**, *8*, 393.
(12) Schichtel, T. E.; Binder, K. *Macromolecules* **1987**, *20*, 1671.
(13) Brochard-Wyart, F. C. *FCR Acad. Sci. Ser. II (Fr.)* **1987**, *305*, 657.
(14) Hess, W.; Akcasu, A. Z. *J. Phys. (Fr.)* **1988**, *49*, 1261.
(15) Kehr, K. W.; Binder, K.; Reulein, S. M. *Phys. Rev. B* **1989**, *39*, 4891.
(16) Binder, K.; Sillescu, H. In *Encyclopedia of Polymer Science and Engineering*, 2nd ed.; Kroschwitz, J. L., Ed.; Wiley: New York, in press.
(17) Gilmore, P. T.; Falabella, R.; Laurence, R. L. *Macromolecules* **1980**, *13*, 880.
(18) Garbella, R. W.; Wendorff, J. H. *Makromol. Chem., Rapid Commun.* **1986**, *7*, 591.
(19) Jones, R. A. L.; Klein, J.; Donald, A. M. *Nature* **1986**, *321*, 16.
(20) Composto, R. J.; Mayer, J. W.; Kramer, E. J.; White, D. *Phys. Rev. Lett.* **1986**, *57*, 1312.
(21) Murschall, U.; Fischer, E. W.; Herkt-Maetzky, Ch.; Fytas, G. *J. Polym. Sci., Polym. Lett. Ed.* **1986**, *24*, 191.
(22) Composto, R. J.; Kramer, E. J.; White, D. M. *Nature* **1987**, *328*, 234.
(23) Brereton, M. G.; Fischer, E. W.; Fytas, G.; Murschall, U. *J. Chem. Phys.* **1987**, *87*, 5048.
(24) Fytas, G. *Macromolecules* **1987**, *20*, 1430.
(25) Kanetakis, J.; Fytas, G. *J. Chem. Phys.* **1987**, *87*, 5048.
(26) Jordan, A. E.; Ball, R. C.; Donald, A. M.; Fetters, L. J.; Jones, R. A. L.; Klein, J. *Macromolecules* **1988**, *21*, 235.
(27) Garbella, R. W. Dissertation Thesis, Darmstadt, FRG, 1987, unpublished.
(28) Higgins, J. S.; Fruitwala, H. A.; Tomlins, P. E., preprint.
(29) Jud, K.; Kausch, H. H. *Polym. Bull.* **1979**, *1*, 697.
(30) Flory, P. J. *Principles of Polymer Chemistry*; Cornell University Press: Ithaca, NY, 1953.
(31) Koningsveld, R.; Kleintjens, L. A.; Nies, E. *Croat. Chim. Acta* **1987**, *60*, 53.
(32) De Groot, S. R.; Mazur, P. *Nonequilibrium Thermodynamics*; North Holland: Amsterdam, 1962.
(33) Crank, J. *The Mathematics of Diffusion*, 2nd ed.; Clarendon Press: Oxford, 1975.
(34) Howard, E.; Lidiard, A. B. *Rep. Progr. Phys.* **1964**, *27*, 161.

(35) Sariban, A.; Binder, K. *J. Chem. Phys.* **1987**, *86*, 5859.
(36) Sariban, A.; Binder, K. *Macromolecules* **1988**, *21*, 711.
(37) Sariban, A.; Binder, K. *Colloid Polym. Sci.* **1988**, *266*, 389.
(38) Baumgärtner, A.; Heermann, D. W. *Polymer* **1986**, *27*, 1777.
(39) Kron, A. K. *Polym. Sci. USSR* **1965**, *7*, 1361.
(40) Wall, F. T.; Mandel, F. *J. Chem. Phys.* **1975**, *63*, 4592.
(41) Rouse, P. E. *J. Chem. Phys.* **1953**, *21*, 1272.
(42) Kremer, K.; Binder, K. *Comput. Phys. Rep.* **1988**, *7*, 259.
(43) Carmesin, I.; Kremer, K. *Macromolecules* **1988**, *21*, 2819. Carmesin, I.; Kremer, K. In *Polymer Motion in Dense Systems*; Richter, D., Springer, T., Eds.; Springer: Berlin, 1988. Carmesin, I.; Kremer, K. *J. Phys. (Paris)* **1990**, *51*, 915.
(44) Baumgärtner, A. In *Applications of the Monte Carlo Method in Statistical Physics*; Binder, K., Ed.; Springer: Berlin, 1984; Chapter 5.
(45) Kehr, K. W.; Binder, K. in *Applications of the Monte Carlo Method in Statistical Physics*; Binder, K., Ed.; Springer: Berlin, 1984; Chapter 6.
(46) Binder, K.; Heermann, D. W. *Monte Carlo Simulation in Statistical Physics: Introduction*; Springer: Berlin, 1988.
(47) Stauffer, D. *Introduction to Percolation Theory*; Taylor and Francis: London, 1985.